A validated model of in vivo electric field distribution in tissues for electrochemotherapy and for DNA electrotransfer for gene therapy

Damijan Miklavčič [a], Dejan Šemrov [a], Halima Mekid [b], Lluis M. Mir [b],*

[a] *University of Ljubljana, Faculty of Electrical Engineering, Trzaška 25, SI-1000 Ljubljana, Slovenia*
[b] *LPPMB, UMR 8532 CNRS, Institute Gustave-Roussy, 39 rue Camille Desmoulins, F-94805 Villejuif Cedex, France*

Abstract

Permeabilising electric pulses can be advantageously used for DNA electrotransfer in vivo for gene therapy, as well as for drug delivery. In both cases, it is essential to know the electric field distribution in the tissues: the targeted tissue must be submitted to electric field intensities above the reversible permeabilisation threshold (to actually permeabilise it) and below the irreversible permeabilisation threshold (to avoid toxic effects of the electric pulses). A three-dimensional finite element model was built. Needle electrodes of different diameters were modelled by applying appropriate boundary conditions in corresponding grid points of the model. The observations resulting from the numerical calculations, like the electric field distribution dependence on the diameter of the electrodes, were confirmed in appropriate experiments in rabbit liver tissue. The agreement between numerical predictions and experimental observations validated our model. Then it was possible to make the first precise determination of the magnitude of the electric field intensity for reversible (362 ± 21 V/cm, mean $\pm$ S.D.) and for irreversible (637 ± 43 V/cm) permeabilisation thresholds of rabbit liver tissue in vivo. Therefore the maximum of induced transmembrane potential difference in a single cell of the rabbit liver tissue can be estimated to be 394 ± 75 and 694 ± 136 mV, respectively, for reversible and irreversible electroporation threshold. These results carry important practical implications. © 2000 Elsevier Science B.V. All rights reserved.

Keywords: Electroporation; Electropermeabilization; Electrode; Electrochemotherapy; Gene therapy; DNA electrotransfer; Finite element modelling

1. Introduction

In the last 2 years, promising results for a new non-viral efficient gene therapy have been obtained in in vivo DNA electrotransfer studies [1–8]. It is also important to note that, recently, drug delivery using electric pulses has entered an active period of clinical trials [9–13]. These two new therapeutical approaches are based on cell electropermeabilisation, also termed electroporation, a phenomenon where a transiently increased plasma membrane permeability is obtained after the cells were exposed to short and intense electrical pulses. Electropermeabilisation thus allows otherwise non-permeant molecules to enter the cytosol [14,15].

For effective drug delivery and gene transfection in vivo, the knowledge of electric field distribution is of utmost importance, to obtain an effective permeabilisation as well as to maintain the viability of the electropermeabi-

lised cells. Indeed, in order to achieve electropermeabilisation in the tissue of interest, the magnitude of electric field intensity has to be above a critical threshold value [14,16,17], i.e. the reversible threshold. Furthermore, the magnitude of electric field intensity should not exceed the value which would produce irreversible damage to the plasma membrane, i.e. the irreversible threshold. Thus, the magnitude of electric field intensity should be high enough to cause reversible electropermeabilisation, but lower than the value causing irreversible damage [2,18]. The latter is the most critical for in vivo gene transfer, but is also desirable in electrochemotherapy in order not to produce large instantaneous necrosis, which would result in massive tumour necrosis and possible ulceration and wound appearance. Moreover, for gene therapy, it has been recently reported [19] that, under relatively homogeneous exposure conditions [20], the optimal conditions for gene transfer correspond to the use of long pulses (20 ms) at a voltage just necessary to obtain cell electropermeabilisation, i.e. just above the reversible permeabilisation threshold. Above the irreversible permeabilisation threshold, when permanent damage is inflicted on the plas-

────────────

* Corresponding author. Fax: +33-1-4211-5276;
E-mail: luismir@igr.fr

ma membrane, viability is lost and efficacy of the DNA transfer is severely impaired [2]. Therefore it was necessary to determine (1) the electric field distribution in the target tissues, (2) the reversible as well as (3) the irreversible permeabilisation thresholds in order to use voltages and electrode geometries resulting in optimal exposure of the targeted tissue to electric fields intensities comprised between the two thresholds.

Very few studies have dealt with these questions. In ex vivo experiments, using two parallel plates separated by 2 mm, that represents a rather homogeneous exposure system, a variable threshold (ranging from 300 to 500 V/cm) was found for a fibrosarcoma tumour exposed to eight pulses of 100 ms at a frequency of 1 Hz [21]. Recently, using a numerical two-dimensional model for electric field distribution, parallel plates as electrodes, and a quantitative Cr^{51}-EDTA uptake assay, threshold for reversible in vivo permeabilisation of mouse skeletal muscle was found at 450 V/cm for the same type of pulses [20]. This work also revealed that the field generated by needle electrodes was not homogeneous and that both the numerical two-dimensional model as well as a global uptake assay were not precise enough, using needle electrodes, for detailed three-dimensional studies of the field distribution in vivo and for threshold determinations. Thus it was necessary to build a detailed three-dimensional model to go further in the understanding and optimisation of electrochemotherapy and gene electrotransfer in vivo.

It seemed also necessary to use new permeabilisation tests giving topological information on electropermeabilisation occurrence with respect to electrode positioning. Therefore a new test was set to perform our work (H. Mekid et al., in preparation) based on the rapid morphological changes produced by the entry of bleomycin into the electropermeabilised cells [22,23].

Needle electrodes seem to be the most practical type of electrodes for clinical applications of both electrochemotherapy and DNA electrotransfer for gene therapy. However, the field generated by two or more needles is very inhomogeneous, as compared to the field distribution between two parallel plates. Nevertheless, it has been previously demonstrated that electric field distribution in the tissue can be controlled by the position of the electrodes in the tissue [24–26]. It was also shown that electrode geometry influences electric field distribution in the tissue and this parameter was taken into account when the work here reported was prepared.

For effective drug delivery after electric pulse application, all the authors have consistently used the same conditions (six or eight pulses of variable voltage-to-distance ratio (usually 1300 V/cm) and of 100 μs delivered at a frequency of 1 Hz) as initially determined by Mir et al. [27]. For in vivo DNA electrotransfer for gene therapy purposes, the electrical parameters have not yet been homogenised: in particular, electric pulse length may vary from 100 μs to 10, 20 or even 50 ms [1–8,28,29]. Therefore,

when it was necessary to fix the experimental conditions for the validation of our tri-dimensional numerical model, the most representative conditions were chosen, i.e. those already used in the clinical settings for electrochemotherapy (pulses of 100 μs). Finally, voltages at which effective either drug delivery or gene electrotransfer were obtained for a given electrode geometry have been determined in vivo [1–4,21,30–32], but until now, the determination of the threshold magnitudes of electric field intensity for reversible and irreversible electropermeabilisation in tissue has not been reported. To find the ways for precise determinations of these thresholds was also one of the objectives of this paper.

Thus, in the present article, we report the construction of a three-dimensional finite element model in order to determine electric field distribution around and between needle electrodes for a homogeneous and isotropic tissue. The results obtained by the numerical model were then tested in liver tissue in in vivo conditions using parameters widely used in clinical applications (eight electric pulses of 100 μs delivered at 1 Hz). In the numerical model, liver was represented as a parallelepiped of homogenous and isotropic conductor. We used two parallel needles as electrodes and studied the influence of electrode diameter on electric field distribution. Both reversible and irreversible electropermeabilisation thresholds for normal rabbit liver cells in vivo were experimentally determined using qualitative tests that allow to visualise the actual geometry of the electric field in vivo and to validate our numerical model.

2. Materials and methods

2.1. Animals

New Zealand white rabbits (Elevage Scientifique des Dombes, Romans, France) were maintained under standard conditions with laboratory diet and water ad libitum. Altogether, 22 rabbits were used in this study. All procedures were carried out under general anaesthesia using intravenous ketamine hydrochloride (Ketamine, Parke Davis, Courbevoie, France) and xylazine 2% (Rompun, Bayer, Puteaux, France). At the end of the experiment, rabbits were killed by an intravenous overdose of Pentobarbital (Sanofi Santé Nutrition Animale, Libourne, France). The experiments were conducted in accordance with the European Council directives and the French legislation concerning animal welfare.

2.2. Electrical treatment

The rabbits were anaesthetised and a subxyphoid incision was performed to expose the liver. Liver tissue local electroporation was performed by inserting two parallel needle electrodes and applying eight rectangular mono-

phasic pulses of 100 μs at 1 Hz repetition frequency. Electric pulses were delivered by an electropulsator PS15 (Jouan, St. Herblain, France) and voltage and current were monitored during the treatment. The electrodes of either 0.3, 0.7 or 1.1 mm diameter (30G1/2, 22G and 19G) separated by insulating template were introduced in the liver perpendicularly to its surface. The depth of penetration was 7 mm. The inner distance between the two electrodes was 8.0 mm.

2.3. Three-dimensional finite element model

A three-dimensional model of liver was built using MSC/EMAS (Electro-Magnetic Analysis System) software package (trademark of The MacNeal-Schwendler, Los Angeles, CA) as a parallelepiped of $32 \times 32 \times 17$ mm as shown schematically in Fig. 1. The liver was represented as a homogenous and isotropic material. If the volume conductor is homogenous and isotropic, then solving Laplace's equation $\nabla^2 u = 0$, which is a partial differential equation of elliptic type. Laplace equation, together with two types of boundary conditions, describes electric field inside the volume conductor. The two types of boundary conditions are: the Dirichlet boundary condition defined as a fixed scalar electric potential, i.e. a fixed applied voltage on the surface of the model, and the Neumann boundary condition defined as the first derivative of the scalar electric potential in the direction normal to the boundary surface of the model, i.e. current density flowing in/out of the model in the direction normal to the surface, divided by the conductivity of the tissue.

Laplace's equation can be solved analytically or using one of the numerical methods. The analytic method is suitable when the geometry, inhomogeneities and anisotropies of the volume conductor are describable in the same co-ordinate system, i.e. Cartesian, spherical or cylindrical. Models in which this condition is not fulfilled result in complicated systems of equations which are difficult to solve. The majority of numerical methods, on the other hand, allow approximation of any geometry, material properties, and boundary conditions. Most methods also allow definition of various material inhomogeneities and in some methods anisotropies can be defined. Complex geometry, inhomogeneities and anisotropies of the tissue are characteristic properties of most of the biological systems. The use of numerical techniques is therefore more appropriate in such studies.

The finite element method, which we used, has proven to be very effective in numerous computations of the electric field inside biological systems [24,26]. The resulting three-dimensional model was made of 6880 three-dimensional finite elements. The meshing was more dense around the electrodes in order to overcome the difference in dimensions of the electrode diameters compared to their mutual distance and outer dimensions of the model. Different electrode sets (i.e. diameters) were modelled by ap-
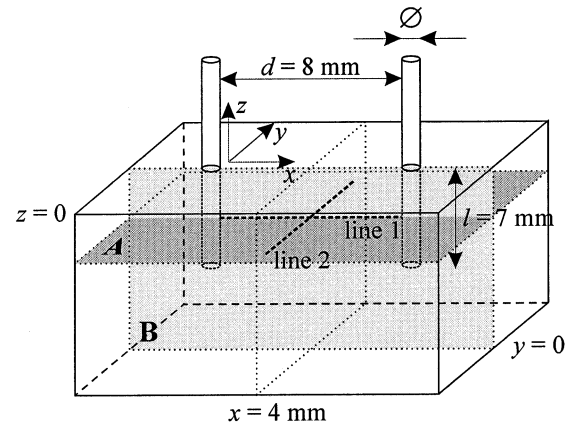

Fig. 1. Schematic presentation of the geometry of a finite element liver model with coordinates, lines and planes of interest. Depth of electrode penetration, $l = 7$ mm; distance between the electrodes, $d = 8$ mm; diameter of the electrodes, $\varnothing = 0.3$, 0.7 and 1.1 mm; line 1 (x, 0–8 mm; $y = 0$ mm, $z = -3.5$ mm); line 2 (y, -4 to $+4$ mm; $x = 4$ mm, $z = -3.5$ mm); plane A, $z = -3.5$ mm; plane B, $y = 0$ mm.

plying appropriate boundary conditions in the grid points corresponding to each of the electrodes. Fixed values of scalar electric potential, i.e. Dirichlet boundary conditions, were assigned to grid points in the regions where electrodes were inserted. Different dimensions of the electrodes were modelled according to the dimensions of the electrodes used in the in vivo study (0.3, 0.7 and 1.1 mm diameter). Potentials of 0 and 100 V were assigned to the sets of grid points representing the two electrodes. Since the model was linear the results were then scaled with the ratio between the exact voltage used in the in vivo experiments and 100 V. On the remaining outer surface of the model, a Neumann boundary condition was applied. This boundary was representing the interface between the conductive liver tissue and air (considered as an ideal dielectric with 0 S/m conductivity). Because the conductor was linear and isotropic, the usual Neumann condition was applied, i.e. the normal derivative of the electric potential on the interface between the model and surrounding air was zero. The electric field was observed in the plane $z = -3.5$ mm perpendicular to the electrodes and in the plane $y = 0$ connecting the immersed electrodes, as depicted in Fig. 1. In addition, electric field was observed along the line 1 connecting the two electrodes ($x = 0$ to 8 mm) at the depth of 3.5 mm, i.e. at $y = 0$ mm, $z = -3.5$ mm, and along the line 2 ($y = -4$ to $+4$ mm) perpendicular to line 1 at the depth of 3.5 mm, i.e. at $x = 4$ mm, $z = -3.5$ mm.

2.4. Irreversible threshold determination

The experimental protocols described below were set and optimised in preliminary experiments. For irreversible threshold determination, 3–4 locations per lobe were usually chosen in the three largest liver lobes and were carefully marked on paper drawings. In the first rabbits, which

served to determine the appropriate range of voltages and voltage increment, electrical treatment was performed with electrodes of 0.7 mm diameter at different voltages ranging from 800 to 1440 V. In three rabbits, the same electrodes were applied to all of the locations using different voltages. Each of the electrodes (diameter 0.3, 0.7 and 1.1 mm, i.e. 30G1/2, 22G and 19G) were used in one rabbit. In addition, different diameter electrodes and different voltages (approximately 860, 960, 1060 and 1360 V) were applied in the same rabbit. That experiment was repeated three times. The voltages were chosen based on numerical model calculations and on the results obtained in first rabbits. After 3 days, the rabbits were killed as at the time that the necrosis produced was visible and no fibrosis, indicative of tissue rearrangements, was yet observed. The liver was removed, visually observed to determine the locations of electrical treatment and cut to pieces so that each contained a single region of interest around the electrodes position. Each of these pieces was then cut at a depth of approximately 3 mm parallel to the liver surface where electrodes were inserted. The liver pieces were then fixed in Bouin's fixative and later embedded in paraffin, cut at a 5 μm thickness by microtome (Microm, Germany) and stained with haematoxylin and eosin. The liver slices were mounted on slide mounts with glass and projected by a slide projector. The areas of tissue necrosis were drawn on the paper in a blind manner by persons who were not involved in any part of this study and had no knowledge on electric field distribution in tissue. The contours of necrotic regions were then scanned and introduced into the computer for further scaling and processing.

2.5. Reversible threshold determination

Bleomycin (Laboratoire Roger Bellon, Neuilly-sur-Seine, France) was injected as a bolus intravenous dose of 50 mg/kg in 2 ml of sterile 0.9% NaCl. This dose was the maximum tolerated dose in rabbits. The positioning of the electrodes was marked by immersing the electrodes in Indian ink before inserting them into the liver. Two parallel needle electrodes of 0.7 mm diameter at inner distance of 8 mm between them were inserted into the liver perpendicularly to the liver surface. Four different locations in each of the three largest liver lobes were used. At the different locations different voltages were applied from 344 (minimum) to 800 V (maximum) at increasing steps of approximately 50 V. All the treatments were performed within 4–20 min after the intravenous injection of bleomycin, thus assuring that electroporation was performed at high concentration of bleomycin in the liver as determined previously. The same experiment was performed in three rabbits. After the treatment was finished, the rabbits were killed, the liver was removed and cut to pieces in a way that each of the pieces contained a single region of interest around the electrodes position. Each of

these pieces was cut at a depth of approximately 3 mm parallel to the liver surface where the electrodes were inserted. After being cut, pieces were fixed in Bouin's fixative and processed for histological examination. The time between electroporation and fixing was between 40 (minimum) and 44 min (maximum). This time has been previously observed to be more than sufficient to observe the characteristic features of bleomycin induced apoptotic-like cell death at the doses used. The liver pieces were then embedded in paraffin, cut at a thickness of 5 μm by microtome (Microm, Germany), stained with hematoxylin and eosin and mounted on microscopic cover glass. The nuclei morphology was examined by two independent observers in regions close to the position of the electrodes and in the middle between the electrode insertion sites. The nuclei were observed for chromatin condensation under the light microscope using $100\times$ objective.

2.6. Hepatocyte diameter determination

The size of the hepatocytes was determined from histological sections by means of a camera lucida mounted on the microscope (Zeiss, Jena, Germany) using objective $100\times$. The largest diameter of a cell was determined, and the one perpendicular to it. The mean diameter of the two was taken in consideration. The diameters of a total of 150 cells were determined from three different histological sections in areas where no changes in nuclei morphology were observed.

3. Results

3.1. Hepatocyte diameter determination

The inner distance between the electrodes was determined in histological sections based on Indian ink marks and was found to be 7.9 ± 0.8 mm. Since the two needles used as electrodes were separated by 8 mm (see Section 2), this experimentally determined value demonstrated that no significant distortion of the sample was caused by handling of tissue samples during preparation for histological observation. Consequently, much confidence could be put on the topological observations made on the histological sections (see below).

Moreover, this validation allowed us to obtain a reliable value of hepatocytes diameter. The diameter of the cells, determined as described in Section 2, was 21.8 ± 2.7 μm. This value is in very close agreement with the hepatocyte diameter determined in other studies performed on rat liver [33].

3.2. Electric field distribution

Numerical calculations were performed for all three electrode diameters (0.3, 0.7 or 1.1 mm) in a way that
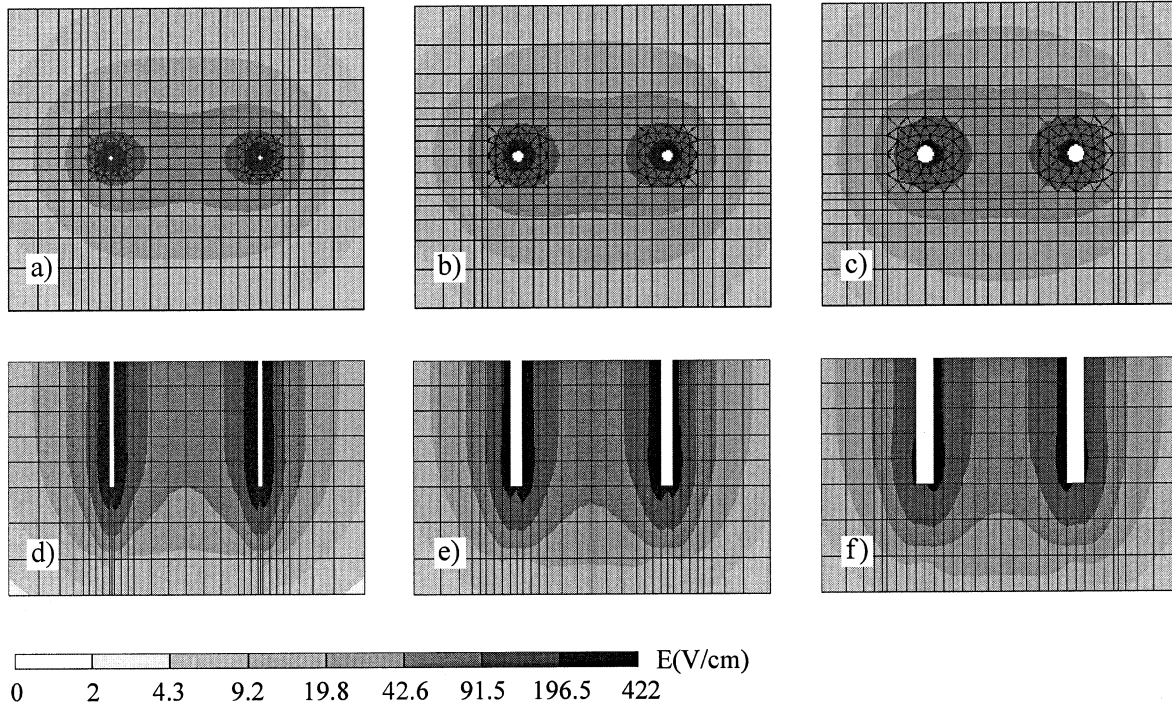
Fig. 2. Electric field intensity (V/cm) at 100 V applied to the electrodes in a section around electrodes of different diameters in the plane A ($z = -3.5$ mm) perpendicular to the electrodes (a, $\varnothing = 0.3$ mm; b, $\varnothing = 0.7$ mm; c, $\varnothing = 1.1$ mm) and in plane B ($y = 0$) along the electrodes (d, $\varnothing = 0.3$ mm; e, $\varnothing = 0.7$ mm; f, $\varnothing = 1.1$ mm).

one of the electrodes was set to 0 V and the other one at 100 V. The results of electric field intensity are thus given in V/cm for 100 V applied. Corresponding values of electric field intensity at actual voltages applied in in vivo experiments were then calculated by multiplying the results with the ratio between the in vivo used voltage and 100 V. This was possible since the model was linear.

In Fig. 2a–c, the electric field distribution around the electrodes is presented in plane A ($z = -3.5$ mm) for all three diameters of electrodes. In all cases, the electric field intensity has the highest value at the electrodes and decreases rapidly with the distance from the electrodes. The decrease of electric field intensity in the vicinity of the

electrodes is steeper at smaller diameters of the electrodes and the area covered with a given or higher electric field intensity is smaller at smaller diameters of electrodes. The electric field distribution was also observed in the plane B ($y = 0$) which goes along the inserted electrodes and is perpendicular to the plane A. Electric field distribution in this plane for all three diameters of electrodes is given in Fig. 2d–f. Similarly, as in the plane A, the highest values of electric field were found around the electrodes in all three cases. The electric field drops rapidly with the distance away from the electrodes. The drop is steeper when electrodes with smaller diameter were modelled. It is also visible that the area covered with given or higher electric
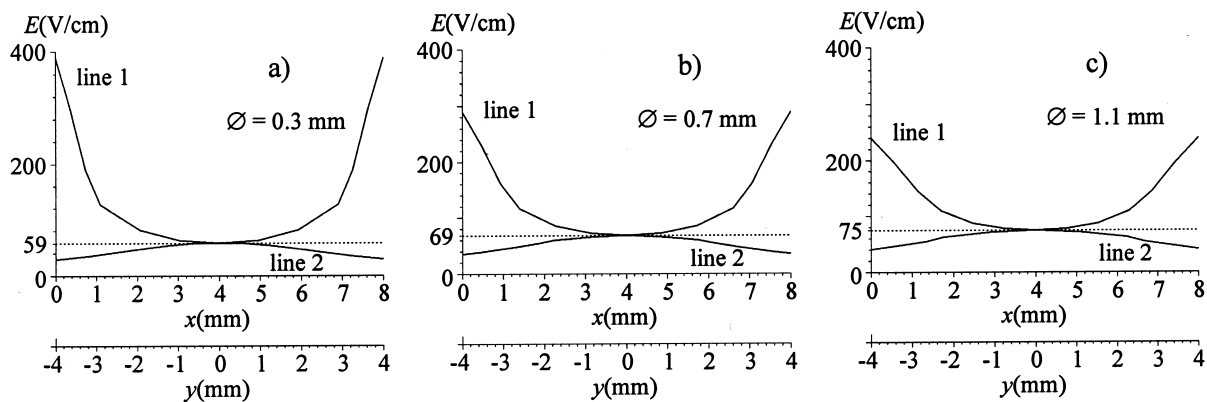

Fig. 3. Electric field intensity at 100 V applied to the electrodes along the line 1 (x, 0– 8 mm, $y = 0$ mm, $z = -3.5$ mm) connecting the two electrodes at the depth of $z = 3.5$ mm (upper trace) and along the line 2 (y, −4 to +4 mm, $x = 4$ mm, $z = -3.5$ mm) perpendicular to the line 1 at the same depth (lower trace) for different electrode diameters (a, $\varnothing = 0.3$ mm; b, $\varnothing = 0.7$ mm; c, $\varnothing = 1.1$ mm).

field intensity is smaller in electrodes with smaller diameter. In particular, the depth on the vertical line between the electrodes ($x = 4$, $y = 0$ mm), parallel to them at which predetermined magnitude of electric field intensity was obtained, was smaller for 0.3 mm electrodes than for 0.7 and 1.1 mm electrodes (Fig. 2d–f). For example, the electric field higher or equal to 42.6 V/cm (at applied 100 V) in the centre between the electrodes reaches the depth of 7 mm in the case of 0.3-mm-diameter electrodes, 8 mm in the case of 0.7-mm-diameter electrodes and 8.5 mm in the case of 1.1-mm-diameter electrodes.

The electric field intensity along the line 1 connecting the two electrodes at the depth of 3.5 mm (x: 0 to 8 mm, $y = 0$ mm, $z = -3.5$ mm) was more precisely examined for all three electrode diameters (Fig. 3). It appeared that the highest electric field intensity was at the surface of the electrodes and was 388, 289 and 239 V/cm for electrodes of diameter 0.3, 0.7 and 1.1 mm, respectively. The lowest value of the electric field intensity was in the middle between the electrodes at $x = 4$ mm and was 59, 69 and 75 V/cm for electrodes of diameter 0.3, 0.7 and 1.1 mm, respectively. When moving away from the middle point between the electrodes on the line 1 ($x = 4$ mm, $y = 0$ mm, $z = -3.5$ mm) outwards along the line 2 (from $y = 0$ mm to $y = -4$ or $+4$ mm), electric field further decreases to 29, 36 and 41 V/cm for electrodes of diameter 0.3, 0.7 and 1.1 mm, respectively. Thus, the highest electric field in the immediate vicinity of the electrodes was obtained in the smallest diameter electrodes, whereas the highest electric field (the lowest minimum) in the centre between the electrodes was obtained with the largest diameter electrodes. Electric field intensity was further decreased when moving from the centre between the electrodes outwards along line 2. This was the case in all diameter of electrodes.

In summary, according to that description, the electric field has a saddle-type shape. For any predetermined electric field intensity, the model allows the calculation of a contour as if the saddle was cut at a given value of electric field intensity (Fig. 4 and 5, numerical data).

3.3. Model validation: correlation between the numerical model and tissue necrosis

In the first experiments on in vivo rabbit liver tissue, at high voltages, necrosis was evident around the electrodes and in the volume comprised between the electrodes 3 days after the pulses application. The extent of necrosis was found to depend on the field strength applied and on the electrode diameter. As described in Section 2, for the irreversible threshold determination, histological sections of liver pieces, cut at the depth of approximately 3–3.5 mm perpendicular to the insertion of the electrodes (plane A) were mounted on the slide mounts and contours of necrosis were drawn in a blind manner. These contours were then compared to the contours of threshold electric
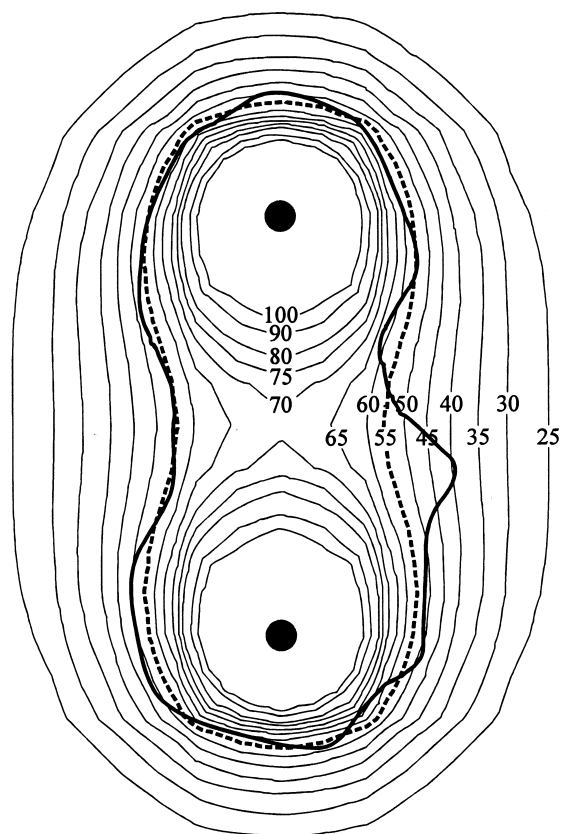

Fig. 4. The distribution of electric field around $\varnothing = 0.7$ mm electrodes at the depth of 3.5 mm (plane A) at 100 V applied. The contours connecting the same electric field intensity are drawn by solid lines and electric field intensity is given in V/cm. Thick solid line is representing the edges of necrosis obtained from histological section of rabbit liver tissue from irreversible threshold determination experiment where 1144 V were applied to 0.7 mm diameter electrodes. Dashed line contour corresponds to the 55 V/cm at 100 V applied, which corresponds to 630 V/cm (i.e. approximately the threshold for irreversible electroporation) at 1144 V applied in the in vivo experiment.

field intensity obtained by numerical modelling at the corresponding diameter of the electrodes (Fig. 4). A very good correlation was found between numerical (see above) and experimental contours, that both were actually dependent on the electrode diameter. For example, Fig. 5 shows the correspondence between the experimental contours of necrosis at the same voltage and the three different electrode diameters with respect to the corresponding calculated contours of 637 V/cm for the three electrodes: necrosis contours drawn by uninformed independent observers fit well with the calculated contours.

In an additional experiment, the livers were cut along the insertion line of electrodes (plane B) in order to verify the electric field distribution in this plane, denoted as plane $y = 0$ mm in numerical model. The electric treatment was performed at different locations in the liver using electrodes of 0.3, 0.7 and 1.1 mm diameter and applying 1104, 968 and 888 V, respectively. The voltage was chosen so that in all three different diameter electrodes the electric field was approximately 650 V/cm in the middle between

the electrodes at $x = 4$ mm, $y = 0$ mm, $z = -3.5$ mm, which is slightly higher than the determined irreversible threshold. In all liver pieces, the necrosis between the electrodes was observed at different depths (data not shown) as predicted by the numerical calculations shown in Fig. 2d–f.

All these observations validated our three-dimensional model.

3.4. Irreversible electropermeabilisation threshold

The irreversible threshold determination was based on the in vitro observations that (at a given number of pulses, given pulse duration and sufficiently high electric field intensity) permanent damage is inflicted on the plasma membrane and therefore loss of cell viability above that threshold is observed. Increase in voltage results in increase of cell death. Tissue necrosis was therefore observed in the liver between the electrodes. Irreversible electropermeabilisation threshold was first determined based on visual examination of freshly cut liver pieces 3 days after the electrical treatment. The exact threshold voltages were determined later, more precisely, based on the macroscopic observation of tissue necrosis in histological sections. The voltage was incrementally increased and the first voltage at which the necrosis was observed in the whole area between the electrodes (including the centre point between the electrodes, i.e. $x = 4$ mm, $y = 0$ mm, $z = -3.5$ mm) was considered to be the threshold voltage. For a given electrode diameter (e.g. 0.7 mm), no necrosis was observed in the middle region between the electrodes below this voltage (1029 ± 53 V for the 0.7 mm electrodes). Above this voltage, however, necrosis was repeatedly observed in the middle region between the electrodes. In addition, the higher the voltage applied, the larger was the area of necrosis around the electrodes which was expected, based on numerical calculations (Fig. 2). This observation was valid for all diameters of the electrodes (Table 1). However, the threshold in the applied voltage depended on the diameter of the electrodes but, according to the numerical calculations, the resulting values of the electric field threshold at the centre point ($x = 4$, $y = 0$, $z = -3.5$ mm) were much closer (Table 1). Based on these voltage determinations and model calculations, electric field irreversible threshold was found as being equal or less than 637 ± 43 V/cm (mean $\pm$ S.D. $n = 9$). The example reported in Fig. 5 to
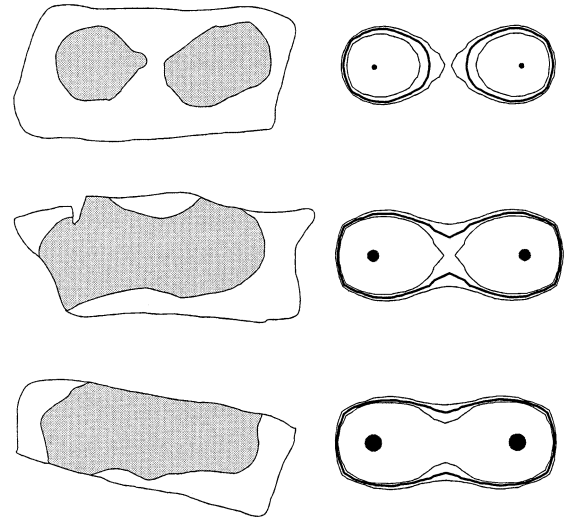

Fig. 5. Contours of necrotic regions (left column) as obtained in in vivo irreversible threshold determination experiments using the same voltage, i.e. 960 V with 0.3 mm (upper row) and 0.7 mm (middle row) diameter electrodes and 952 V (lower row) with 1.1 mm diameter electrodes. In the right column, the contours of irreversible threshold (thick line) $\pm$ standard deviation (thin line), i.e. 637 ± 43 V/cm are given as calculated for the voltages applied using the electrodes with same diameter.

show the agreement between the numerical and the experimental contours was also in agreement with that value of the irreversible threshold. Indeed, at the applied voltage in the experiment reported in Fig. 5 (960 V), the electric field intensity at the middle point between the electrodes at the depth of 3.5 mm ($x = 4$ mm, $y = 0$ mm, $z = -3.5$ mm) is 568, 652 and 714 V/cm for electrodes of 0.3, 0.7 and 1.1 mm diameter, respectively. As shown in Fig. 5, the same voltage papplied produced tissue necrosis in the whole area between the electrodes when electrodes of 0.7 and 1.1 mm diameter were used, but not when electrodes of 0.3 mm were used, confirming the threshold value (637 ± 43 V/cm).

3.5. Reversible electropermeabilisation threshold

For the experimental determination of the reversible electropermeabilisation threshold, electric treatment was performed in the presence of a high concentration of bleomycin which induces an apoptotic-like cell death [22] resulting in clear morphological changes in cell nuclei, i.e.

Table 1
Determination of threshold voltages U (V) by macroscopic examination of tissue necrosis in histological sections and calculated corresponding electric field intensity E (V/cm) at the centre point between the electrodes ($x = 4$ mm, $y = 0$ mm, $z = -3.5$ mm)

Diameter (mm)	Rabbit 1		Rabbit 2		Rabbit 3		mean $\pm$ S.D.
	U (V)	E (V/cm)	U (V)	E (V/cm)	U (V)	E (V/cm)	U (V)
0.3	968	571	1056	623	1064	628	1029 ± 53
0.7	952	657	856	591	960	662	927 ± 58
1.1	856	642	952	714	872	654	893 ± 51

Pooled value of electric field intensity (which is independent of electrode diameter) from all nine determinations in the three rabbits. $E = 637 \pm 43$ V/cm (mean $\pm$ S.D.; $n = 9$).
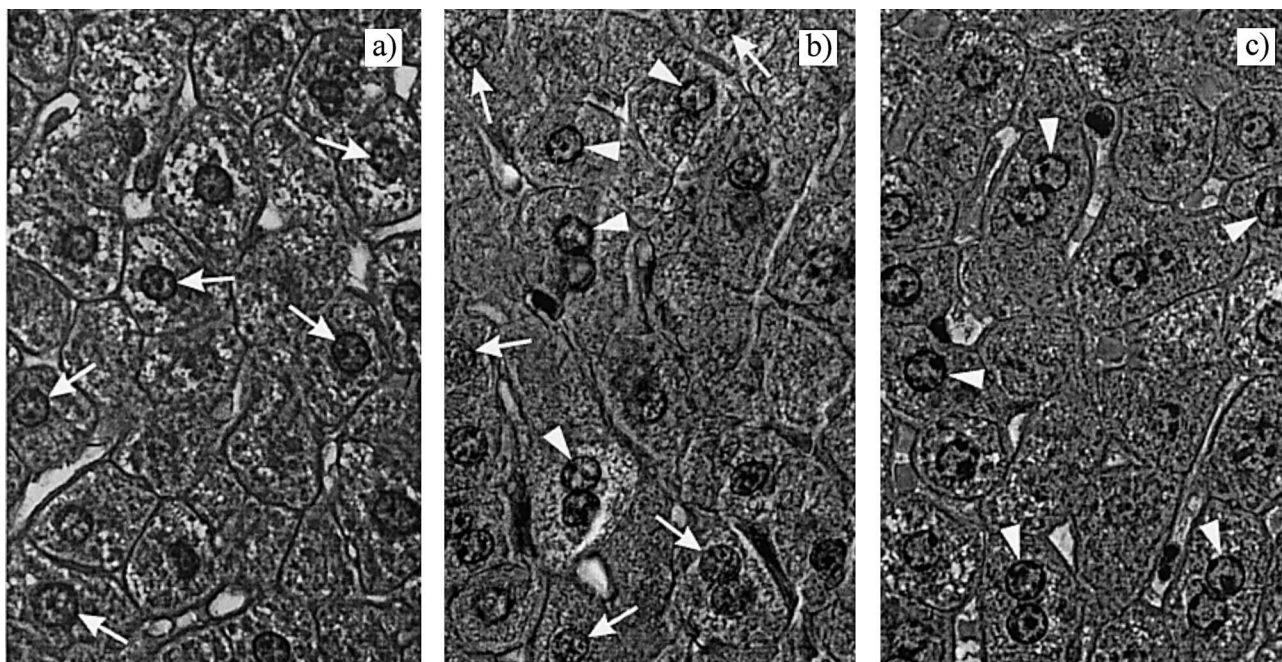
Fig. 6. Haematoxylin and eosin stained histological sections from 0.7-mm-diameter electrodes applying 500 V (a), 544 V (b) and 640 V (c) which corresponds to the electric field magnitude in the middle between the electrodes at the depth of approximately 3 mm, of 343, 374 and 440 V/cm, respectively. (a) Unaltered nuclei in the middle region between the needles at electric field below the reversible threshold. (b) Altered, i.e. apoptotic, and unaltered nuclei in the middle region between needles at electric field approximately at the reversible threshold. (c) Altered, i.e. apoptotic nuclei in the middle region between electrodes at electric field above the threshold. Arrows point at normal nuclei, while arrowheads indicate apoptotic-like nuclei with chromatin condensation. Observations were made under a light microscope using $100\times$ objective.

chromatin condensation, already 30 min later [23]. Electric treatment was performed in three rabbits at 12 locations in each rabbit. At each of the locations a different voltage was applied with 0.7 mm diameter needle electrodes with the inner distance of 8 mm between them. The microscopic observation of nuclei morphology in the middle region between the two electrode insertion sites was performed by two independent observers.

The observation revealed that nuclei appeared normal, i.e. no chromatin condensation was observed, at voltages equal or lower than 500, 496 and 440 V in the three rabbits. At 544, 544 and 492 V, respectively, normal and altered nuclei were found next to each other in the observed middle region. At voltages equal or higher than 592, 592 and 536 V, respectively, all the nuclei were altered. At the higher voltages, the alterations were more pronounced. Interestingly, even at the lowest voltages employed, apoptotic changes were observed in the vicinity of the electrodes, and at the highest voltages employed, the largest part of the histological sections displayed altered nuclei. These observations are well in accordance with the calculated electric field distribution at $z = -3.5$ mm. The threshold voltage therefore was determined to be equal or lower than 527 ± 30 V (mean $\pm$ S.D.), which results in the electric field intensity of 362 ± 21 V/cm at the centre point between the electrodes ($x = 4$ mm, $y = 0$ and $z = -3.5$ mm) based on the results of the calculated electric field distribution. No changes in nuclei morphology were observed in the control sections which were exposed to the same

bleomycin concentration and processed in the same way as the electropulsated sections except for the electric pulse delivery. In Fig. 6, examples are given where 0.7 mm diameter electrodes were used at 500 V (Fig. 6a), 544 V (Fig. 6b) and 640 V (Fig. 6c) which results in electric field intensity of 343 V/cm (i.e. below the threshold), 374 V/cm (i.e. approximately at the threshold value) and 440 V/cm (i.e. above the threshold), respectively. The corresponding nuclei morphology reveals normal cell nuclei at electric field intensity below the reversible threshold (Fig. 6a), apoptotic nuclei, i.e. showing chromatin condensation, at the electric field intensity above reversible threshold (Fig. 6c), and the simultaneous presence of normal and apoptotic cell nuclei in the centre point between the electrodes ($x = 4$ mm, $y = 0$ mm, $z = -3.5$ mm) at the threshold (Fig. 6b).

4. Discussion

We report here the first determinations of in vivo permeabilisation thresholds and the corresponding transmembrane voltages at these thresholds based on three-dimensional model of electric field distribution in liver, and the corresponding biological experimental observations that validated the three-dimensional model. The model predicted, and the in vivo experiments confirmed, that electric field distribution depended on the diameter of the electrodes (Fig. 2). Electrodes with smaller diameter produced

more inhomogeneous electric field distribution, as expected (Fig. 2 and 3). To obtain the same electric field intensity in the centre point between the electrodes, different voltage needs to be applied when electrodes of different diameter are used. The smaller the diameter of the electrodes, the higher the voltage that has to be applied to obtain the same electric field intensity in the centre point between the electrodes. When using two needle electrodes separated by 8 mm, in order to obtain an over-threshold electric field in the targeted liver tissue (including the centre point between the electrodes), and reversibly permeabilise the liver cells, it is necessary to apply voltages of 614, 525 and 483 V or higher for 0.3-, 0.7- and 1.1-mm electrode diameters, respectively.

This model was validated by direct comparison of the geometry of the contours, i.e. lines joining all the points in which the electric field has the same intensity (obtained with electrodes of different diameters), with the experimental contours (using identical electrode diameters) of the necrosis resulting from permanent damage inflicted on liver cells by fields of an intensity equal to or above the irreversible permeabilisation threshold. Rabbit liver tissue was considered as isotropic and homogenous tissue with respect to its specific electric conductivity and was modelled as homogenous and isotropic conductive parallelepiped. This could represent a limitation to our study because different inhomogeneities are present in the liver tissue resulting, for example, from the presence of vessels which can distort the electric field distribution. Nevertheless, the experimental validation of that model allowed us to use the numerical calculations of electric field distribution and the biological observations in in vivo experiments to determine the values of the threshold electric field intensities for reversible (362 ± 21 V/cm) and irreversible (637 ± 43 V/cm) electropermeabilisation of rabbit liver tissue in vivo using eight pulses of 100 μs delivered at the frequency of 1 Hz.

The determination of the hepatocyte average diameter, which showed a relatively homogeneous size, allowed us to calculate the induced transmembrane voltage at the two thresholds. Indeed, it is known that, when a cell is exposed to an external electric field, a transmembrane voltage is induced which, for a single spherical cell can be determined according to equation $\Delta U = fRE \cos\vartheta$ (where ΔU is the induced transmembrane potential, f is a numerical factor, which under idealised conditions equals 1.5) [34], R is the radius vector of the cell, E is the electric field intensity and ϑ is the angle between the cell radius vector and the electric field vector). However, this equation is only valid for a single cell in a homogenous electric field: if multiple cells are observed in the space, the induced transmembrane voltage depends on their density [35]. In the case where the cells are densely packed, the induced transmembrane voltage is lower. Based on previous calculations, the maximum induced transmembrane voltage for densely packed cells (i.e. tissue) in close connection (but

with no electrical connections between cells) can be estimated by the same equation where $f = 1$ [35]. Therefore, for hepatocytes of 21.8 ± 2.7 μm diameter, the induced threshold transmembrane voltage therefore, is 372 ± 75 and 694 ± 136 mV, for reversible and irreversible electroporation threshold values of electric field intensity as measured in the present study in vivo in rabbit liver tissue. This is the first determination of the induced transmembrane voltages at the corresponding permeabilisation thresholds for cells in liver.

Indeed, the only tissue electropermeabilisation threshold determinations to which our results can be compared with were reported by Belehradek and co-workers in 1994 [21] and by Gehl and co-workers in 1999 [20]. In both cases, authors used the same pulse parameters (eight pulses of 100 μs delivered at 1 Hz) than those used in the work reported here. However, only reversible permeabilisation thresholds were determined in these studies. Moreover, the induced transmembrane voltages at the threshold were not evaluated: in the study by Belehradek et al. [21], the irregular diameter of the LPB tumour cells was not measured in the tumour, and in the study by Gehl et al. [20], the work on the skeletal muscle did not allow secure determinations because of the differences in diameter between muscle fibres and even along the same muscle fibre. In individual isolated mammalian muscle cells, the transmembrane potential was calculated by Bier et al. [36] to be between 340 and 480 mV at the reversible electropermeabilisation threshold, and 540 mV or higher at the irreversible (or, as termed by these authors, stable) electropermeabilisation threshold. For the induced transmembrane potential calculations, they used the value of $f = 1.5$. In their experiments, however, the electric field was perpendicular to the long axis of the myotube, for which case the factor f would be more close to the value $f = 2$ (the case of an isolated cylinder in electric field). By taking this into account and recalculating their results, induced transmembrane potential would be between 453 and 640 mV at reversible permeabilisation threshold, and 720 mV at irreversible threshold. It also needs to be stressed that they determined the permeabilisation by using a single pulse of 4 ms duration and observing Mg^{2+} influx. Irrespective of that, the values they reported are in very good agreement with the values of induced transmembrane potential as determined in our study.

In Belehradek and co-workers study [21], electric field intensity for reversible permeabilisation was also determined ex vivo in tumour slices using bleomycin. Moreover, as tumour slices 2 mm thick were placed between two parallel plate electrodes, the electric field intensity can be justifiably approximated by the voltage-to-distance ratio. The reversible permeabilisation threshold was found to be in the range between 300 and 500 V/cm. In Gehl and co-workers study [20], a two-dimensional model for electric field distribution was built, and according to this model and the experimental values, the reversible threshold

(probably that of the largest fibres in the treated muscle) was obtained for an electric field of 450 V/cm (with the electric field direction perpendicular to the long axis of the muscle). Since calculations based on two-dimensional models tend to overestimate the electric field, this value could be even lower. In spite of large differences in the cells' shapes and dimensions, and in the tissue structure (for example, contrary to liver cells, muscle fibres are not connected by gap junctions), similar electric field was necessary to obtain the reversible permeabilisation and thus reversible threshold was of similar intensity for all these tissues. The reasons for this similarity are still unknown. It is noteworthy that these values are lower than the usual permeabilisation thresholds for cells exposed in vitro to the same type of pulses (eight pulses, 100 μs, 1 Hz). For example, it was already shown that, using the same electrodes and the same cells either in suspension or forming a tissue (tumour), the electric field intensity required for reversible permeabilisation threshold drops from 700 V/cm (cells in suspension) to 300–500 V/cm (cells in tissue) [21]. This drop cannot be explained by the calculated modification of the factor f from 1.5 to 1 discussed here above. Other parameters, like the average number of gap junctions between the cells in the tissue [21,37,38] could influence the permeabilisation of cells in the tissues. This shows again that investigations on parameters affecting cell electropermeabilisation in vivo are further warranted.

This also means that previous in vitro determinations of transmembrane voltage at the reversible permeabilisation threshold may be of limited use for comparisons with in vivo determinations. In one of the early review papers [14] a 150–500-mV transmembrane potential was reported as being reached to obtain the membrane permeabilisation. Hibino and co-workers reported higher values of transmembrane voltage needed for cell electroporation, being in the range of 1000 mV [39]. An experimental evaluation of electroporation voltage in cells by Teissié and Rols [40] yielded about 200 mV as the electroporation transmembrane voltage for many different cell systems. Kakorin et al. [41] also determined electroporation transmembrane voltage for salt-filled lipid bilayer vesicles which was 530 mV under their experimental conditions [41]. All the determinations which were reported hitherto were done on single cells and vesicles, or on cells and vesicles in suspension. Moreover authors used different pulse parameters, different cells and different permeabilisation test molecules, all of which affect the threshold [42,43]. Therefore direct comparisons are not entirely warranted. Nevertheless, the reversible threshold transmembrane voltage determined by us, based on in vivo tissue permeabilisation using numerical modelling and taking into account cell density, falls within determinations reported by other authors.

The value of our approach lies in combining the numerical modelling and biological experimentation. The topological validity of the model was assessed through an ex-

cellent correlation between biological observations and numerical calculations obtained with electrodes of different diameters electrodes (Figs. 4 and 5). It is important to note, in the perspective of the development of new electrodes for DNA electrotransfer in vivo or for electrochemotherapy of tumours in patients, that the voltages at which alterations in nuclei morphology (histological determination of the reversible threshold) and tissue necrosis (macroscopic determination of the irreversible threshold) were observed, depended on the diameter of the electrodes used in the experiments. Briefly, when the electrodes of smaller diameter were used, the voltages at which tissue permeabilisation was obtained were higher both for the reversible and for the irreversible electropermeabilisation, and electric field distribution was less homogeneous. These observations have important practical consequences for electrochemotherapy of liver tumours in the clinical situation, and of other visceral tumours for which needle electrode applicators have already been developed [32,44], as well as for the gene therapy by means of DNA electrotransfer. In particular, the numerical values determined with the experimental work carried out here using eight pulses of 100 μs and 1 Hz are important for the design of electrodes for electrochemotherapy because all the current clinical protocols of electrochemotherapy use such short pulses of 100 μs [9–13].

For gene therapy using DNA electrotransfer, a new approach which is rapidly developing [1–8], the model remains valid, but the numerical values of the reversible and irreversible thresholds would be different. Both thresholds depend on pulse characteristics. Indeed, if the reversible threshold for the skeletal muscle in mice was 450 V/cm when eight pulses of 100 μs were delivered at 1 Hz [20], it has been shown that, to achieve optimal DNA electrotransfer using the same electrodes on the same tissue, long pulses of at least 20 ms were necessary [6], and with these long pulses, reversible threshold for the skeletal muscle in mice was found to be close to 80 V/cm only [19]. Therefore, for gene therapy purposes in liver tissues, it will be necessary to determine the respective reversible and irreversible thresholds for 20-ms-long pulses. Then these values could be introduced in the model here reported to find the optimal electric field amplitude that will achieve the permeabilisation of the vast majority of the treated liver tissue without inducing toxic effects.

References

[1] M.P. Rols, C. Delteil, M. Golzio, P. Dumond, S. Cros, J. Teissié, Nat. Biotechnol. 16 (1998) 168–171.

[2] L.M. Mir, M.F. Bureau, R. Rangara, B. Schwartz, D. Scherman, C.R. Acad. Sci. Paris 321 (1998) 893–899.

[3] H. Aihara, J. Miyazaki, Nat. Biotechnol. 16 (1998) 867–870.

[4] T. Suzuki, B.C. Shin, K. Fujikura, T. Matsuzaki, K. Takata, FEBS Lett. 425 (1998) 436–440.

[5] R.L. Harrison, B.J. Byrne, L. Tung, FEBS Lett. 435 (1998) 1–5.

[6] L.M. Mir, M.F. Bureau, J. Gehl, R. Rangara, D. Rouy, J.-M. Caillaud, P. Delaere, D. Branellec, B. Schwartz, D. Scherman, Proc. Natl. Acad. Sci. USA 96 (1999) 4262–4267.

[7] I. Mathiesen, Gene Ther. 6 (1999) 508–514.

[8] G. Rizzuto, M. Cappelletti, D. Maione, R. Savino, D. Lazzaro, P. Costa, I. Mathiesen, R. Cortese, G. Ciliberto, R. Laufer, N. LaMonica, E. Fattori, Proc. Natl. Acad. Sci. USA 96 (1999) 6417–6422.

[9] R. Heller, M.J. Jaroszeski, D.S. Reintgen, C.A. Puleo, R.C. DeConti, R.A. Gilbert, L.F. Glass, Cancer 83 (1998) 148–157.

[10] G. Serša, B. Štabuc, M. Čemažar, B. Jancar, D. Miklavčič, Z. Rudolf, Eur. J. Cancer 34 (1998) 1213–1218.

[11] L.M. Mir, L.F. Glass, G. Serša, J. Teissie, C. Domenge, D. Miklavčič, M.J. Jaroszeski, S. Orlowski, D.S. Reintgen, Z. Rudolf, M. Belehradek Jr., R. Gilbert, M.P. Rols, J. Belehradek, J.M. Bachaud, R. DeConti, B. Štabuc, M. Čemažar, P. Coninx, R. Heller, Br. J. Cancer 77 (1998) 2336–2342.

[12] Y. Kubota, L.M. Mir, T. Nakada, I. Sasagawa, H. Suzuki, N. Aoyama, J. Urol. 160 (1998) 1426.

[13] W.R. Panje, E. Harrell, M.P. Hier, A. Goldman, G.R. Garman, I. Bloch, Ann. Otol. Rhinol. Laryngol. 107 (1998) 779–785.

[14] T.Y. Tsong, Biophys. J. 60 (1991) 297–306.

[15] S. Orlowski, L.M. Mir, Biochim. Biophys. Acta 1154 (1993) 51–63.

[16] K. Kinosita Jr., I. Ashigawa, N. Saita, H. Yoshimura, H. Itoh, K. Nagayama, A. Ikegami, Biophys. J. 53 (1988) 1015–1019.

[17] J. Weaver, Y.A. Chizmadzhev, Bioelectrochem. Bioenerg. 41 (1996) 135–160.

[18] M. Danfelter, P. Engström, B.R.R. Persson, L.G. Salford, Bioelectrochem. Bioenerg. 47 (1998) 97–101.

[19] J. Gehl, L.M. Mir, Biochem. Biophys. Res. Comm. 261 (1999) 377–380.

[20] J. Gehl, T.H. Sørensen, K. Nielsen, P. Raksmark, S.L. Nielsen, T. Skovsgaard, L.M. Mir, Biochim. Biophys. Acta 1428 (1999) 233–240.

[21] J. Belehradek Jr., S. Orlowski, L.H. Ramirez, G. Pron, B. Poddevin, L.M. Mir, Biochim. Biophys. Acta 1190 (1994) 155–163.

[22] O. Tounekti, G. Pron, J. Belehradek Jr., L.M. Mir, Cancer Res. 53 (1993) 5462–5469.

[23] O. Tounekti, J. Belehradek Jr., L.M. Mir, Exp. Cell Res. 217 (1995) 506–516.

[24] D. Miklavčič, K. Beravs, D. Šemrov, M. Cemazar, F. Demšar, G. Serša, Biophys. J. 74 (1998) 2152–2158.

[25] G. Serša, M. Čemažar, D. Šemrov, D. Miklavčič, Bioelectrochem. Bioenerg. 39 (1996) 61–66.

[26] D. Šemrov, D. Miklavčič, Comput. Biol. Med. 28 (1998) 439–448.

[27] L.M. Mir, S. Orlowski, J. Belehradek Jr., C. Paoletti, Eur. J. Cancer 27 (1991) 68–72.

[28] A.V. Titomirov, S. Sukharev, E. Kristanova, Biochim. Biophys. Acta 1088 (1991) 131–134.

[29] R. Heller, M. Jaroszeski, A. Atkin, D. Moradpour, R. Gilbert, J. Wands, C. Nicolau, FEBS Lett. 389 (1996) 225–228.

[30] R. Heller, M. Jaroszeski, J. Leo-Messina, R. Perrot, N. Van Voorhis, D. Reintgen, R. Gilbert, Bioelectrochem. Bioenerg. 36 (1995) 83–87.

[31] G. Serša, M. Čemažar, D. Miklavčič, Cancer Res. 55 (1995) 3450–3455.

[32] R.A. Gilbert, M.J. Jaroszeski, R. Heller, Biochim. Biophys. Acta 1334 (1997) 9–14.

[33] V. Raicu, T. Saibara, H. Enzan, A. Irimajiri, Bioelectrochem. Bioenerg. 47 (1998) 333–342.

[34] T. Kotnik, F. Bobanovič, D. Miklavčič, Bioelectrochem. Bioenerg. 43 (1997) 285–291.

[35] R. Susil, D. Šemrov, D. Miklavčič, Electro. Magnetobiol. 17 (1998) 391–399.

[36] M. Bier, S.M. Hammer, D.J. Canaday, R.C. Lee, Bioelectromagnetics 20 (1999) 194–201.

[37] E. Fear, M. Stuchly, IEEE Trans. Biomed. Eng. 45 (1998) 856–866.

[38] E. Fear, M. Stuchly, IEEE Trans. Biomed. Eng. 45 (1998) 1259–1271.

[39] M. Hibino, H. Itoh, K. KinositaJr, Biophys. J. 64 (1993) 1789–1800.

[40] J. Teissie, M.P. Rols, Biophys. J. 65 (1993) 409–413.

[41] S. Kakorin, S.P. Stoylov, E. Neumann, Biophys. Chem. 58 (1996) 109–116.

[42] M.P. Rols, J. Teissié, Biophys. J. 75 (1998) 1415–1423.

[43] M. Čemažar, T. Jarm, D. Miklavčič, A. Maček Lebar, A. Ihan, N.A. Kopitar, G. Serša, Electro. Magnetobiol. 17 (1998) 263–272.

[44] L.H. Ramirez, S. Orlowski, D. An, G. Bindoula, R. Dzodic, P. Ardouin, C. Bognel, J. Belehradek Jr., J.-N. Munck, L.M. Mir, Br. J. Cancer 77 (1998) 2104–2111.